**Advances in cartilage repair: the influence of inorganic clays to improve mechanical and healing properties of antibacterial Gellan gum-Manuka honey hydrogels**

Maria A. Bonifacio[a*], Andrea Cochis[b*], Stefania Cometa[c], Annachiara Scalzone[d], Piergiorgio Gentile[d], Giuseppe Procino[e], Serena Milano[e], Alessandro C. Scalia[b], Lia Rimondini[b§], Elvira De Giglio[a§]

[a] Department of Chemistry, University of Bari "Aldo Moro", via E. Orabona 4, Bari, 70126, Italy

[b] Department of Health Sciences, University of Piemonte Orientale UPO, Center for Translational Research on Autoimmune and Allergic Diseases (CAAD), c.so Trieste 15/A, Novara, 28100, Italy

[c] Jaber Innovation s.r.l., via Calcutta 8, Rome, 00144, Italy

[d] School of Engineering, Newcastle University, Stephenson Building, Claremont Road, Newcastle upon Tyne, NE1 7RU, UK

[e] Department of Biosciences, Biotechnologies and Biopharmaceutics, University of Bari "Aldo Moro", via E. Orabona 4, Bari, 70126, Italy

[*] These authors equally contributed to the work.

[§] Co-corresponding authors

**Contacts:**

Elvira De Giglio

Department of Chemistry, University of Bari "Aldo Moro", via E. Orabona 4, Bari, 70126, Italy

elvira.degiglio@uniba.it

Tel./Fax: +39 0805442021

**Abstract**

Effective treatment of cartilage defects represents a challenging problem, mainly due to the tissue's limited intrinsic self-repair capacity; the use of polymeric scaffolds as tissue substitute is rapidly increasing, but it is still limited by poor mechanical properties. Moreover, the onset of an infection can irreversibly affect the healing process. Accordingly, in this work we describe, for the first time, the preparation of composite scaffolds based on gellan gum, antibacterial Manuka honey and an inorganic clay (mesoporous silica, sodium-calcium bentonite or halloysite nanotubes). The surface composition, morphology, mechanical and biological features of such composites are herein assessed, aiming to optimize the composition of a superior scaffold for cartilage repair. Results demonstrated that after 45 days of in vitro incubation with human mesenchymal stem cells, the mesoporous silica-composite hydrogels exhibited significant changes in peak elastic and dynamic moduli over time thus demonstrating superior mechanical properties. Moreover, mesoporous silica provided the best performances in terms of *in vitro* cytocompatibility and antibacterial preventive activity in protection of cells in a co-culture model. Therefore, this selected composition was exploited for subcutaneous implantation in mice to investigate materials biocompatibility and infection prevention. Results demonstrated that composites did not cause severe immune response as well as they were able to restrain the infection. Accordingly, GG-MH-MS composites represent a very promising tool for cartilage tissue engineering.

**Keywords**

Composite hydrogels, gellan gum, inorganic clays, antibacterial, cytocompatibility, cartilage repair.

## 1. Introduction

Articular cartilage injuries represent a widely diffused issue since they mainly affect aging people, but also athletes and teenagers [1,2]. Cartilage ability of spontaneous regeneration is low and, even when substituted with engineered tissues, the regenerative potential still remains clinically sub-optimal. This is due to the resident cells' scarcity and no vascularization, which also result in unsuitable mechanical properties of the scaffold with respect to the functional load [3]. In addition, bacterial contamination of the scaffolds or of the engineered replacement tissue is a frequent side effect, worsened by the lack of

vascularization and the consequent tissue inability to promptly hinder infection [4]. The literature reports many promising attempts to promote cartilage repair overcoming the abovementioned limitations, including the use of cryopreserved chondrocytes as well as cartilage substitutes [5,6] and natural-based materials [7]. In this regard, hydrogel scaffolds are one of the most described in osteochondral tissue engineering, because of their ability to support cells and allow optimal metabolites exchange [8,9]. However, their mechanical features still represent an open question to solve. In our previous work, the addition of Manuka Honey to gellan gum-based hydrogels resulted in improved mechanical properties and intrinsic antibacterial features [10,11]. Moreover, composite scaffolds prepared adding inorganic clays to the polymeric network often lead to significant improvements in material's compressive modulus, morphology and cytocompatibility [12,13]. Indeed, hard inorganic particles can reinforce the soft and flexible polymeric matrix, especially when a homogeneous dispersion and a controllable morphology of the composites are reached. In order to obtain superior mechanical properties, micro- or nano-sized clays (such as Laponite®, montmorillonite, Cloisite15A, etc.) are usually selected in order to avoid particle aggregation, which in turn could represent a trigger point for material breakage [14-16]. In a previous work, gellan gum-based hydrogels were reinforced with halloysite nanotubes (HNT) [10], which can be considered a widely used and well-known cytocompatible clay, able to confer interesting mechanical properties to composites [17].

In this work, gellan gum-based hydrogels were modified, for the first time, with mesoporous silica and with sodium-calcium bentonite. The clays' impact on the new composites' features was evaluated with respect to the bare organic network and to the HNT-modified systems.

The choice of bentonite and mesoporous silica clays, rather than other conventional clays (e.g. talc, mica, calcium carbonate, kaolin etc.), came from the specific properties of the selected clays. Bentonite has a layered structure, with a relatively high cation exchange capacity and high surface area, which could be helpful to intercalate molecules between the lamellae, acting as potential controlled release system [18,19]. Differently from traditional porous silica, mesoporous silica shows highly ordered porosity, with uniform and customizable pore sizes, thanks to the nano-templating synthetic approach [20]. Moreover,

mesoporous silica-reinforced scaffolds were already prepared with other polymers (e.g. chitosan, polyurethane), displaying hierarchically porous architectures suitable for drug delivery [21, 22]. However, the application of such clays in gellan-based composite scaffolds for cartilage regeneration was never afforded, thus requires an accurate evaluation of *in vitro* and *in vivo* performances. A systematic investigation of all the composite scaffolds was carried out through X-ray Photoelectron Spectroscopy, Scanning Electron Microscopy, static compression tests and *in vitro* cytocompatibility studies. The mesoporous silica-reinforced scaffolds showed the best mechanical, morphological and biological performances. Therefore, these scaffolds underwent an additional characterization through *in vitro* chondrogenesis and *in vivo* implantation. Moreover, stress-relaxation tests were also performed before and after chondrogenesis, in order to highlight samples' viscoelastic behavior over long culture periods. Up to 45 days of culture, the silica-enriched scaffolds showed the potential to support cartilage regeneration.

## 2. Materials and methods

### *2.1 Materials and Hydrogels preparation*

Unless otherwise specified, all reagents were supplied by Sigma-Aldrich. Gellan gum is hereafter named GG (Phytagel™, molecular weight 1,000Kg/mol, low acylation degree). Medical grade Manuka honey 12Plus (MH) was purchased by ManukaGuard® (Ndal Manufacturing Industries). As far as the inorganic clays were concerned, mesoporous silica (MS, particle size <150µm, pore size 6nm) and halloysite nanotubes (HNT, $Al_2Si_2O_5(OH)_4 \cdot 2H_2O$, mean length 1-3µm, mean diameter 30-70nm) were purchased from Sigma-Aldrich. Besides, sodium-calcium bentonite (BE) (Bentonite AG/8W) was purchased from Dal Cin SpA. $MgCl_2$ salt, used as cross-linker, was of Redi-dri™ grade. Ultrapure water was obtained by a Milli-Q® Integral system (Millipore-Merck).

Hydrogels were prepared as previously reported for GG-based hydrogels [10,11,23] with some modifications. Briefly, GG powder (2%w/v) was dissolved under stirring in water at 90°C. After cooling the solution at 60°C, MH (2%w/v) was added and vigorously stirred. Clay-reinforced samples were obtained by mixing the dissolved components with an aqueous suspension of MS, HNT or BE (each

0.5%w/v) previously sonicated at 37°C. The gels were then poured in plastic molds and crosslinked through the external gelation method [24] using $MgCl_2$ solutions as cationic source (0.5%w/v). A list of the hydrogel types prepared in this work is reported in Table 1, which also displays the hydrogels' final appearance.

**Table 1. Composition of the systems.** Nomenclature and nominal composition of the prepared hydrogels. All the %w/v are expressed in respect to water. Scale bars: 5mm. Abbreviations: gellan gum (GG), Manuka honey (MH), halloysite nanotubes (HNT), bentonite (BE), mesoporous silica (MS).

| | 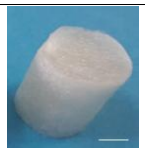 | 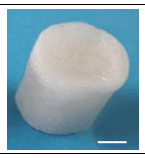 |  |  |
|---|---|---|---|---|
| **Sample code** | **GG-MH** | **GG-MH-HNT** | **GG-MH-BE** | **GG-MH-MS** |
| **GG content (%w/v)** | 2 | 2 | 2 | 2 |
| **MH content (%w/v)** | 2 | 2 | 2 | 2 |
| **Clay content (%w/v)** | 0.5 | 0.5 | 0.5 | 0.5 |

After 24h, the scaffolds were obtained through freezing at -20°C for 24h and consequent freeze-drying for 48h (Christ ALPHA 1-2/LD Plus, Martin Christ, Germany). The duration of the freeze-drying step was optimized for each of the selected inorganic clay, ranging from 10 to 14 hours. Re-hydrated samples underwent mechanical and biological characterizations.

*2.2 Spectroscopic and morphological characterizations*

The dehydrated hydrogels underwent spectroscopic characterization through X-ray Photoelectron Spectroscopy (XPS). Sections of samples were studied in high power mode by a scanning microprobe PHI 5000VersaProbe II (Physical Electronic) with monochromatized AlKα X-ray radiation source. Survey scans and high-resolution spectra were acquired in Fixed Analyzer Transmission (FAT) mode, with pass energy of 117.4eV and 29.35eV respectively. The base pressure during analysis was kept constant at $10^{-9}$ mbar. The MultiPak software package (version 9.9.0) was exploited for data analysis. Normalized peak area was used to calculate atomic percentages, considering empirically derived sensitivity factors of the MultiPak library.

The scaffolds were also studied by Scanning Electron Microscopy (SEM, JSM-5600LV, JEOL) at accelerating voltage of 20kV. The samples were fixed on aluminum stubs using carbon tape and gold-coated using a BIO-RAD Sputter Coater machine. Fiji software (from NIH) was used to calculate sample porosity, considering at least 20 random pores from each of three SEM images. After image thresholding, Fiji's tools to measure the average area and diameter of each pore were exploited [25]. Moreover, the void area percentage was calculated as the percentage ratio of total pore area to the total area. Results were reported as mean ± standard error of the mean.

*2.3 Mechanical characterization: static compression and stress-relaxation test*

Static compression tests were performed using a mechanical testing machine (EZ-SX, Shimadzu) equipped with a 20N load. Five hydrogels for each composition (cylinder-shaped samples with 1.6 cm diameter and 2 cm height) were evaluated at room temperature. The crosshead speed was set at 1 $mm \cdot min^{-1}$, and the load was applied while the specimen was compressed until break (about 35-40% of its original height). The compressive Young's moduli (E) were calculated as the slope of the initial linear portion of the stress–strain curve (0-10%).

Stress-relaxation tests were performed, following the protocol proposed by the authors [10], with a single compression ramp at a speed of $10\% \cdot min^{-1}$ until reaching 10% strain. Then, the strain was held constant for 1000 s, while the load was recorded as a function of time. Within 10% compression, the stresses versus strain relations of the gels were almost linear. The peak stress was obtained at 10% strain. The equilibrium Young's modulus ($E_q$) was determined by the equilibrium load reached after 1000 s of relaxation under unconfined compression. The peak elastic modulus ($E_0$) and $E_q$ are the two parameters calculated for this test. Recorded data were analyzed using MATLAB R2017 software. By fitting a third order exponential decay to the relaxation curves, three relaxation times were acquired, as:

$$\sigma(t) = A \cdot (e)^{-t/\tau_1} + B \cdot (e)^{-t/\tau_2} + C \cdot (e)^{-t/\tau_3} + D$$

where A, B and C are the amplitudes corresponding to the three relaxation times $\tau_1$, $\tau_2$ and $\tau_3$.

*2.4 In vitro cytocompatibility of the hydrogels*

*2.4.1 Human Mesenchymal Stem Cells culture*

Human mesenchymal stem cells (hMSCs) were kindly provided by Prof. P. Genever, University of York. They were isolated from bone marrow, immortalized through hTERT lentiviral vectors (hMSCs Y201) and used for *in vitro* experiments [26]. hMSCs were cultured in low glucose DMEM supplemented with 15% fetal bovine serum (FBS, Sigma-Aldrich, Milan) and 1% antibiotics (penicillin/streptomycin). When hMSCs cells reached 80-90% of confluence, they were detached with trypsin-EDTA and used for *in vitro* evaluations.

*2.4.2 In vitro hMSCs viability and metabolic activity*

Top and bottom surfaces of the dehydrated scaffolds were cut off to expose the internal porous matrix (final height ~10 mm). Scaffolds were sterilized in 100% ethanol for 1h and dried overnight. Samples were treated with or without 200µL of ABM G422 extracellular matrix (ABM®), previously diluted 1:1 in PBS. After a further drying step of 30 min, $25x10^4$ hMSCs were dropwise seeded on top of each scaffold and cultured as reported above in a final volume of 2 mL. Cells-free scaffolds were considered as negative controls while cells seeded onto multiwell plate wells coated with ABM® G422 matrix-PBS (1:1) were used as positive control. After 72h from seeding, the samples were incubated with trypsin-EDTA for 10 min at 37°C to detach hMSCs. Then, the number of viable cells was determined by Burker chamber count using Trypan blue. Results were expressed as percentage over the sample GG-MH. Cells metabolic activity was measured using PrestoBlue™ Reagent (Thermo Fisher Scientific). Briefly, 0,5 mL of cell culture medium containing 10% of PrestoBlue™ Reagent were added to cells and after 1h the absorbance was measured at 570 nm, using FLUOstar Omega microplate reader (BMG Labtech). The absorbance of hMSCs seeded on cell culture wells was considered as the 100% reference.

*2.4.3 In vitro MSCs colonization on dehydrated samples*

Scaffolds were pre-treated and seeded with hMSCs cells as reported in 2.4.2 and cultured for 10 days. Cells were fixed in 4% paraformaldehyde in PBS for 1h at RT and then washed twice with PBS. Samples were incubated with 1µg/mL DAPI in PBS for 20 min and washed twice with PBS. Scaffolds were stored in optimal cutting temperature medium (OCT, Thermo Fisher Scientific) diluted in PBS (1:1) overnight at

4°C. Samples were then infiltrated for 3h with OCT at RT, longitudinally cryosectioned at -20°C and 8µm sections were collected on Superfrost Plus™ microscope slides (Thermo Fisher Scientific). Cell colonization within dehydrated gels was evaluated in sequential images of 5 fields of 2mm ranging from the seeding surface to the bottom surface, to analyze the entire thickness of each hydrogel. Images were obtained with a fluorescence microscope (Leica LMD7000, camera Leica DFC310 FX).

*2.5 In vitro cells-bacteria co-cultures*

*2.5.1 In vitro bacterial growth condition*

Two bacterial strains frequently responsible of joint infections were selected, i.e. *S. aureus* (ATCC 43300) and *S. epidermidis* (clinical isolate, provided by the Clinical Microbiology Unit of Novara Maggiore Hospital, with Patient's informed consent and in full accordance with the Declaration of Helsinki). Bacteria were cultured on selective Mannitol Salt Agar plate (Sintek) until the formation of single round colonies. Then, 2-3 colonies were picked and transferred in 30 mL of Luria-Bertani broth (LB, Sigma-Aldrich) until the optical density of the culture reached 0.001 at 600 nm (Spark spectrophotometer, Tecan Trading AG), equal to a concentration of $1x10^5$ bacteria/mL.

*2.5.2 In vitro antibacterial activity*

Samples were sterilized and pre-treated as described in section 2.4.2. After drying, $25x10^4$ hMSCs were seeded by the drop-on method onto each sample, using antibiotic-free medium (DMEM, 15% FBS) and incubated for 24 h at 37°C, 5% $CO_2$ in order to allow complete attachment. After 24 h, the samples were moved in a new 24-wells plate and infected with 1mL/sample of a suspension containing $1x10^5$ bacteria in DMEM 15% FBS, prepared as previously described. Infected samples were incubated for 48 h at 37°C, 5% $CO_2$ to allow the growth of bacteria and hMSCs. This time-point was selected after evaluating bacteria metabolism in cells medium as shown in Supplementary Figure S1.

After PBS washing, the samples were incubated with trypsin-EDTA (10 min at 37°C) and the number of viable cells was assessed through Trypan blue staining and counting by Burker chamber. Positive controls were set up with hMSCs seeded on the samples, without bacterial infection.

*2.6 In vitro hMSCs chondrogenesis*

Sterile dehydrated specimens were located into a 48-wells plate; then, $4x10^6$ hMSCs cells were resupended into 80µL of a 1:1 DMEM-extracellular matrix (ABM®) to re-hydrate specimens. The scaffolds were maintained into basal medium (DMEM 15% FBS) for 48 h to equilibrate the systems; then, basal medium was replaced by the chondrogenic one, composed of DMEM High Glucose (4.5g/L) supplemented with 10% ITS+1 Premix Tissue Culture Supplement, $10^{-7}$M dexamethasone, 1 µM ascorbate-2-phosphate, 1% sodium pyruvate and 10 ng/mL transforming growth factor-beta 1 (Tgf-β1, all from Sigma-Aldrich). PrestoBlue™ assay was performed after 48 h equilibration and after 21 days differentiation to verify cells metabolism. The scaffolds were cultured for 21 days in chondrogenic medium prior to biological assessment. Chondrogenesis was evaluated by histology and real-time PCR (see Supplementary material). For histological analysis, specimens were cryo-embedded into Kilik (from BioSigma) and 8 µm cryo-slices were stained with Alcian blue, Safranin-O and Sirius red. Chondrogenic (collagen type-II (COL 2), and aggrecan (ACAN), osteogenic/ fibroblastic (collagen type-I (COL 1)) genes expression was evaluated (Table S1). Chondrogenic (collagen type-II (COL 2), and aggrecan (ACAN), osteogenic/fibroblastic (collagen type-I (COL 1)) genes expression was evaluated.

*2.7 In vivo immunological and antibacterial evaluations*

*2.7.1 Subcutaneous infection*

Adult (12 weeks-old) infection-free certified wild type mice were purchased (C57BL/6JOlaHsd, from Envigo). They were stored in the animal enclosure of Novara at the University of Piemonte Orientale following a 12+12h dark/light cycle with a fasten 20-25°C RT. All animal surgical procedures were performed under 3% isofluorane general anesthesia and after local ethical committee and Italian Ministry of Health approval (protocol n. 854/2017-PR). Test materials were evaluated in terms of biocompatibility by means of immunological reaction by subcutaneous implant, as previously described [27] and as a model of non-tissue specific infections [28-29]. Briefly, a skin pocket was surgically created into the dorsal side of mice. Then, 4x4 mm scaffolds were re-hydrated with sterile PBS and immediately inserted into the pocket. Finally, the surgical wounds were sutured with 4.0 VICRYL® suture (polyglactin 910,

Ethicon, Somerville). Analgesic agents were administered by subcutaneous injection of flumequine (Flumexil®) at 0.15 mg/10 g and sodium metamizole (Farmolisine®, CevaVetem Spa) at 0.001 mL/10 g. Animals injected with PBS into the skin pocket were considered as control. Mice were sacrificed after 1 week, by means of carbon dioxide ($CO_2$) under 5% isofluorane-induced general anesthesia.

*2.7.2 In vivo immunological reaction*

Mice were divided into 6 groups composed of 4 animals each: i) control (PBS) without infection, ii) control (PBS) with infection, iii) GG-MH without infection, iv) GG-MH with infection, v) GG-MH-MS without infection and vi) GG-MH-MS with infection. Sterile and re-hydrated specimens were subcutaneously implanted as prior described and maintained for 1 week. Afterwards, mice were sacrificed and spleens collected; the tissues were smashed and passed through a 100 μm filter. After lysis of red blood cells, the pellet was resuspended in PBS supplemented with 3% FBS and the cells were counted. Then, $1x10^6$ cells were stained using specific antibodies after 15 min of saturation (for further details see Supplementary material).

*2.7.3 In vivo antibacterial activity*

Specimens were infected with $1x10^3$ *S. aureus* bacteria/scaffold prior to be subcutaneously implanted as prior described. After 1 week, specimens were collected, carefully separated from surrounding tissues by surgical blades, submerged with 1mL of PBS and finally mechanically minced by forceps. The number of viable colonies was obtained by the CFUs count as prior described [30].

*2.8 Statistical analysis*

In order to assess the statistical significance of porosity measurements, static compression test, *in vitro* cell viability, expression of chondrogenic markers and *in vivo* biocompatibility, one-way ANOVA with repeated measurements and Tukey *post hoc* test was performed using GraphPad Prism 8. Two-way ANOVA with repeated measurements was used to highlight differences between samples after metabolic activity, stress-relaxation test, *in vitro* and *in vivo* antibacterial assessment. Then, Dunnett's test was exploited to compare the impact of the different variability sources. Statistical significance was set at $p < 0.05$.

## 3. Results

### *3.1 Spectroscopic and morphological characterizations*

#### *3.1.1 XPS characterization*

XPS characterization was performed on all the composite hydrogels. Atomic percentages of the elements detected on the surface of both unreinforced and clay-reinforced scaffolds, as well as the Si2p high-resolution spectra of both the clays alone and the same loaded into the hydrogel networks are reported in Fig.1.

| a) Sample | C1s | O1s | Si2p | Al2p | Ca2p | Na1s | Mg2s |
|---|---|---|---|---|---|---|---|
| **GG-MH** | 67,8 | 31,9 | -- | -- | -- | -- | 0,3 |
| **GG-MH-HNT** | 74,4 | 24,9 | 0,2 | 0,3 | -- | -- | 0,2 |
| **GG-MH-BE** | 68,7 | 30,0 | 0,7 | 0,1 | 0,2 | 0,2 | 0,1 |
| **GG-MH-MS** | 52,7 | 45,8 | 1,4 | -- | 0,2 | -- | 0,1 |

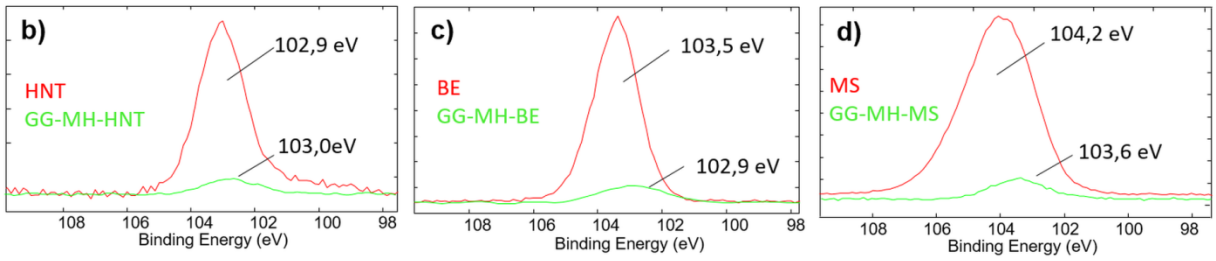


**Figure 1. XPS analysis.** Surface chemical composition of bare and clay-reinforced composite scaffolds (a); comparison of Si2p signals recorded on HNT (b), BE (c) and MS with the respective composites.

#### *3.1.2 Morphological analysis*

SEM analysis was performed to evaluate the effect of inorganic clays on the scaffolds' morphology. All the samples showed a porous architecture, with "open-cell" structures, characterized by a high degree of interconnectivity. The mean pore diameter ranged from 254±151 μm for GG-MH-MS to 531±219 μm for GG-MH (Fig.2). Furthermore, inorganic clays were homogenously distributed within the polymeric matrix in all the samples. Only few agglomerates were detected and the void area ranged from 22.4±0.1% for GG-MH-BE to 52.4±0.5% for GG-MH. Pore walls increased their thickness in GG-MH-MS samples compared to GG-MH-HNT and GG-MH-BE ones.

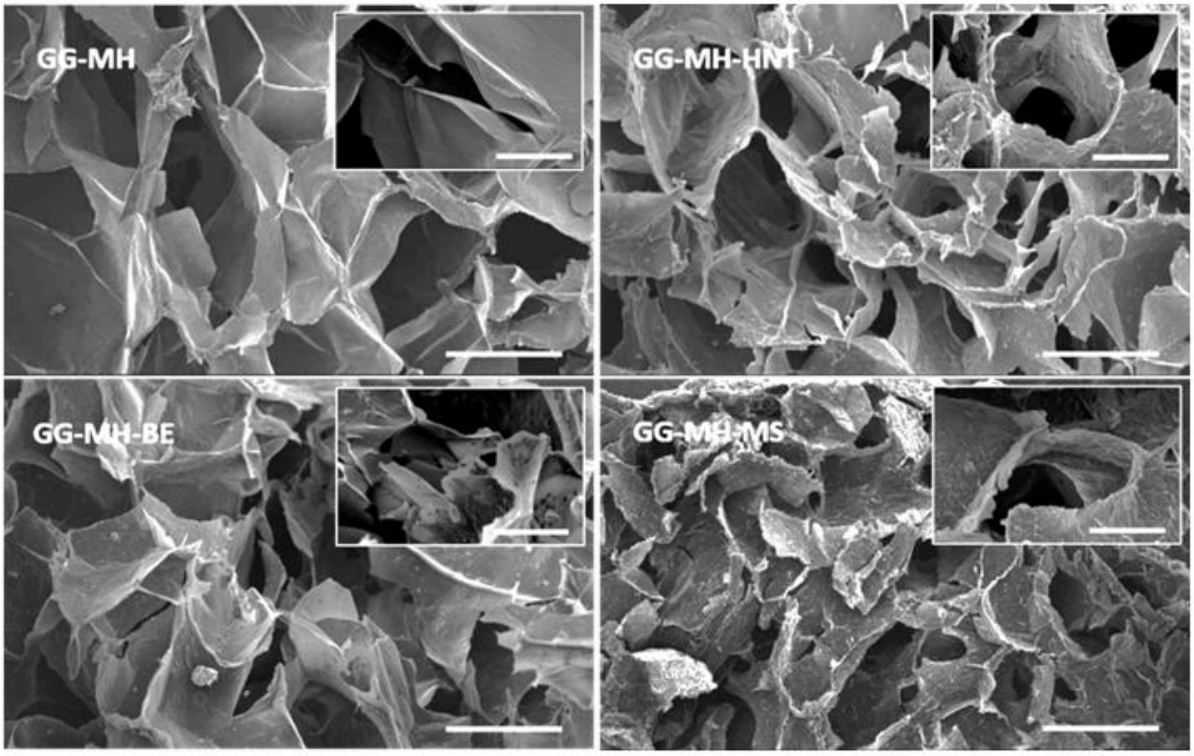


| | Void area % | Mean pore area (μm²) | Mean pore diameter (μm) |
|---|---|---|---|
| **GG-MH** | 52.4±0.5 | 222087±11104 | 531±219 |
| **GG-MH-HNT** | 37.7±0.1[a] | 91330±2826[d] | 306±161 |
| **GG-MH-BE** | 22.4±0.1[b] | 54231±1063[e] | 260±83 |
| **GG-MH-MS** | 30.0±0.3[c] | 83868±2143[d] | 254±151 |

**Figure 2. Morphological characterization.** SEM micrographs of the prepared scaffolds. Scale bars: 500 μm; Inset scale bars: 200 μm. The table reports porosity measurements. Means with different lowercase letters differ significantly.

*3.2 Mechanical characterization: static compression test*

Figure 3 reports the compressive Young's moduli (E) of all the composite samples that were calculated from the slope of the initial linear portion of the compression stress–strain curves. The compressive modulus increased with inorganic clay addition as compared with the bare polymeric hydrogel. E values ranged from 112±9 kPa for GG-MH-BE to 140±25 kPa for GG-MH-MS). These compressive Young's moduli were at least 40% more than the values calculated for GG-MH (86±5 kPa). Furthermore, no significant differences between compressive moduli of all the clay-reinforced samples were observed.

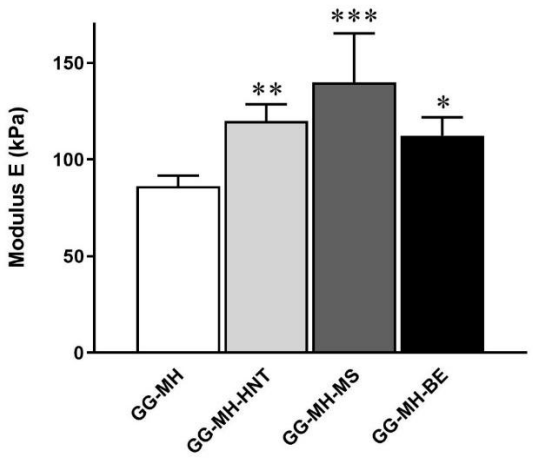


**Figure 3. Compressive Young's moduli obtained from static compression tests.** *p<0.01, **p<0.001, ***p<0.0001.

*3.3 In vitro cytocompatibility of the hydrogels and co-cultures with bacteria*

The *in vitro* cytocompatibility of gellan gum-based hydrogels, prepared with different inorganic clays, was evaluated through viability, metabolic and colonization assays (Fig.4 and Fig.5). The direct count of viable hMSCs after 48 h from seeding is reported in Fig.4a. More viable cells were detected on GG-MH-MS samples as compared to those cultured on GG-MH scaffolds. On the other hand, the addition of BE seemed to impair cell viability, while no significant differences were det

ected between the number of viable cells on GG-MH-HNT and GG-MH samples (Fig.4a). Metabolic activity of hMSCs cells cultured on hydrogels was determined using PrestoBlue™ reagent (Fig.4b). Compared with day 1 after seeding, there was a significant increase of the metabolic activity at day 10 for all the hydrogels, except for GG-MH-BE. At day 1, cells grown on GG-MH-MS showed higher metabolic activity than on GG-MH or GG-MH-HNT. On the other hand, poor results were obtained on GG-MH-BE. Then, hMSCs were *in vitro* co-cultured with *S. aureus* or *S. epidermidis* on each sample type (Fig.4 c and d). Interestingly, GG-MH-MS and GG-MH-HNT scaffolds were able to protect hMSCs from *S. aureus*, as well as from *S. epidermidis* infection. Indeed, thanks to the antibacterial activity of the scaffolds, the number of viable cells was not significantly decreased after infection, showing that the presence of antibacterial molecules was effective in hindering bacteria, preserving cells with a "protective" activity.

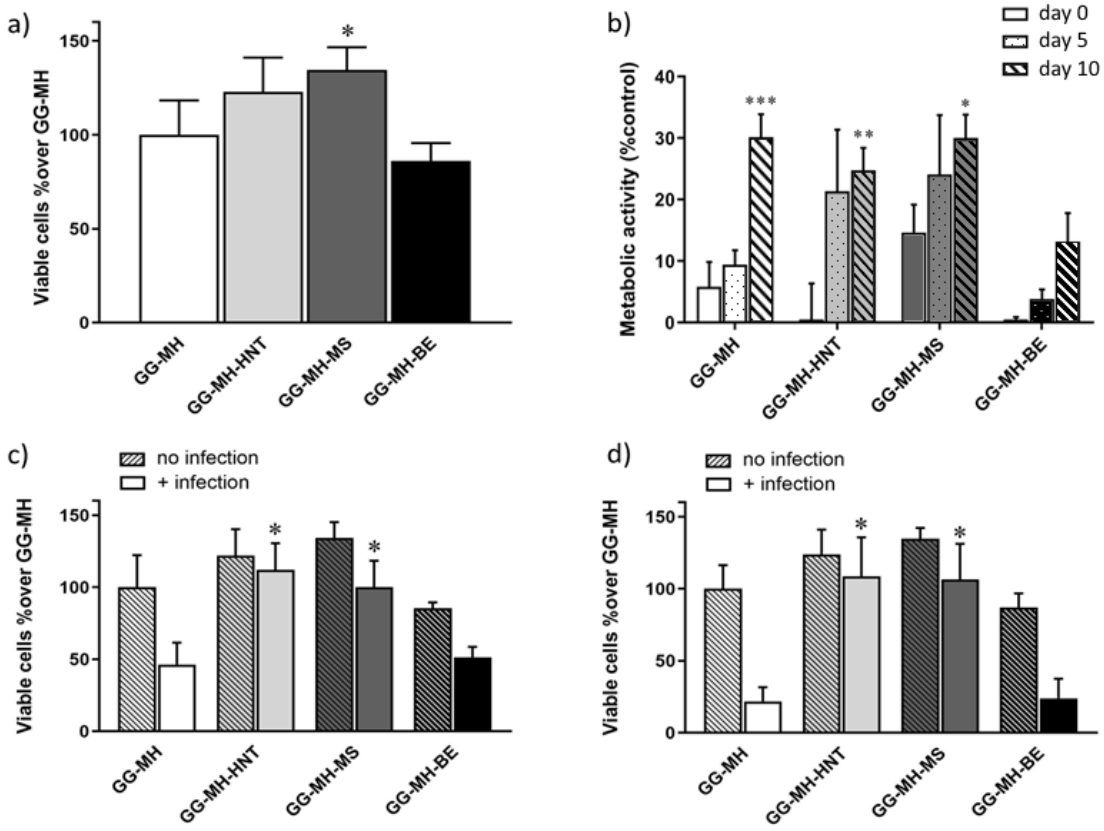


**Figure 4. *In vitro* cytocompatibility.** a) Cell viability assay. Statistical significance refers to viability percentage over GG-MH; b) Metabolic activity assay was performed at 1, 5 and 10 days after seeding, respectively. Results were expressed as percentage of hMSCs cultured on well plates used as control; the statistical analysis is referred to day 1 for each filler. c) hMSCs viability in co-culture with *S. aureus* and d) *S. epidermidis*. In c) and d) statistical significance refers to cell viability over GG-MH in presence of infection. *p<0.01, **p<0.001, ***p<0.0001.

Moreover, it must be taken into account that the metabolic activity assay does not clarify whether cells proliferate on the seeding surface of the scaffold or they reach the scaffold`s depth. In order to shed light on this point, a colonization experiment was performed, showing that hMSCs colonized in depth only GG-MH-MS scaffolds (Fig.5). Briefly, cells nuclei were stained with DAPI and thin cryosections of the scaffolds analyzed under a fluorescent microscope from top (seeding surface) to bottom. Cells seemed to migrate, to different extents, throughout the trabecular matrix. In particular, cells were able to colonize only the upper one fifth of the GG-MH, GG-MH-HNT and GG-MH-BE scaffolds. Strikingly, though, in GG-MH-MS cells migrated and seemed to proliferate in close contact with the internal *trabeculae* of the scaffold reaching the deepest part of it.

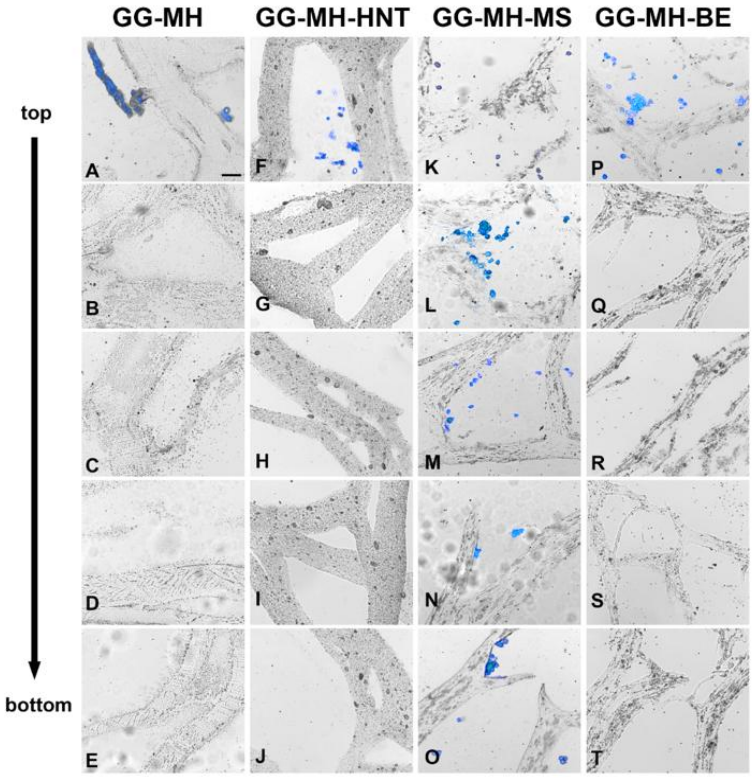


**Figure 5.** ***In vitro*** **colonization assay.** Five sequential observation fields are reported from the top to the bottom of each scaffold block. hMSCs cells were seeded on top of each scaffold and allowed to proliferate for 10 days. Cells nuclei were stained by DAPI (light blue), while the trabeculae of the scaffolds acquired in bright field. Comparable results were obtained in three independent experiments.

*3.4 In vitro hMSCs chondrogenesis*

Fig.6 summarizes the results of 3D chondrogenesis. First of all, hMSCs metabolism was evaluated both after 48 h in basal medium and after 21 days of chondrogenic differentiation. As reported in Fig.6a, a not significant decrease in hMSCs metabolism was observed for GG-MH scaffolds over time. Looking to chondrogenesis analysis, both tested scaffolds effectively supported differentiation. PCR analysis obtained by the $^{\Delta\Delta}$CT calculation (Fig. 6b-d) revealed that hMSCs after 21 days in differentiative medium overexpressed chondrogenic genes COL 2 and ACAN (Fig. 6b and 6c, respectively) while the expression of the osteogenic gene COL 1 did not increase over time (Fig.6d) in comparison with day 0 values. However, ACAN expression was favoured by the clay loading as it resulted as significant in comparison with the control ($p<0.05$, indicated by *). Indeed, histological analysis demonstrated that cells were able to aggregate into scaffold pores (showed in the Fig. 6e-f) and to produce a cartilage-like

matrix rich in glycosaminoglycans (GAGs), as clearly visible by the intense Alcian blue (Fig. 6e-f) and Safranin-O (Fig. 6h) as well as composed by a dense layer of collagen as suggested by the yellow-orange color from the Sirius red staining (Fig. 6g).

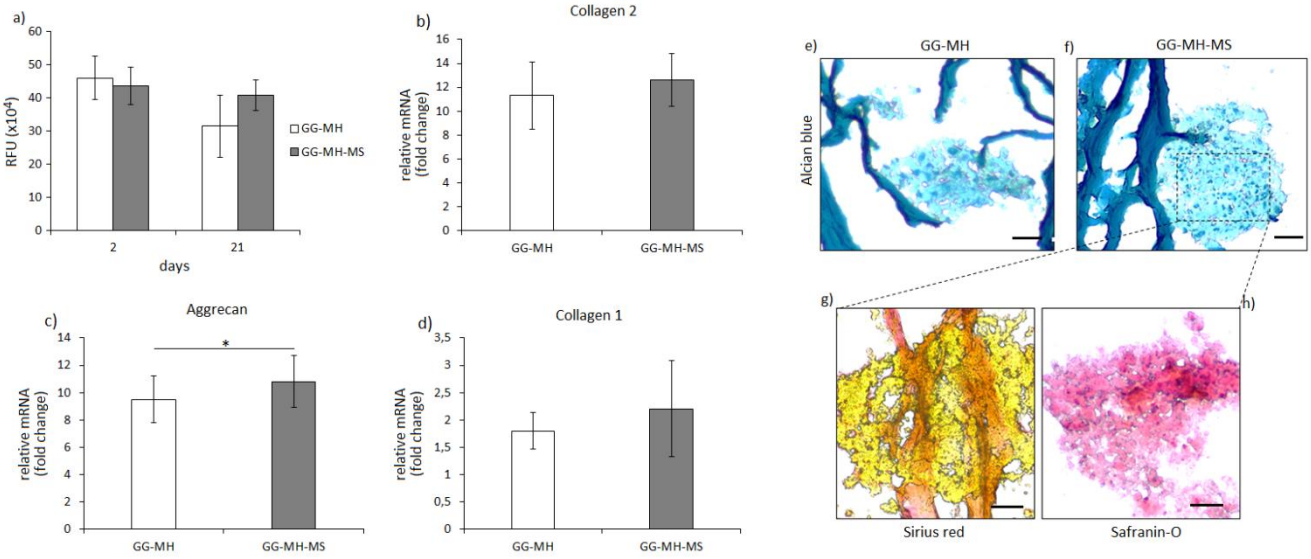


**Figure 6. Chondrogenesis assays.** a) metabolic activity assay, performed after 2 and 21 days of culture, in basal and chondrogenic medium respectively; b-d) chondrogenic genes (collagen 2 and aggrecan) and osteogenic (collagen 1) genes expression; e-f) representative images (Alcian blue) of cells aggregates grown as spheroids inside the scaffold pores; g-h) collagen (Sirius red) and GAGs (Safranin-O) staining of GG-MH-MS. Scale bars: 100μm.

*3.5 Stress-relaxation test before and after in vitro chondrogenesis*

Unconfined stress-relaxation tests were performed in order to evaluate the impact of the newly deposited extracellular matrix on the scaffolds' mechanical properties after *in vitro* hMSCs chondrogenic culture. At time 0 (Fig. 7a), the peak elastic modulus was calculated, following the protocol of Liming Bian et al. [31], obtaining values of 84 ± 6 kPa for GG-MH-MS (Fig. 7b). The equilibrium moduli, strongly influenced by the relaxation "behavior" of the hydrogels under a fixed constrain, were calculated from the equilibrium stress values divided by the 10% strain. $E_q$ reached 42 ± 2 kPa for GG-MH-MS (Fig. 7c). Furthermore, the obtained stress-relaxation curves were analysed using Matlab to fit the experimental values with a third order exponent polynomial equation. The calculated relaxation times were related with the calculated equilibrium moduli and showed the viscoelastic behavior of the hydrogels (Fig. 7d) [10, 23]. Furthermore, after 45 days of *in vitro* incubation with hMSCs cells, the composite hydrogels exhibited significant changes in peak elastic and

dynamic moduli over time, with strong increases between 21 and 45 days. It is noteworthy that the equilibrium modulus of GG-MH-MS hydrogels increased 2-fold (from 42 ± 2kPa at time 0 to 64 ± 4kPa at 15 days and to 93 ± 5kPa at 45 days). Conversely, the mechanical properties of GG-MH hydrogels remained relatively unchanged for the whole culture time.

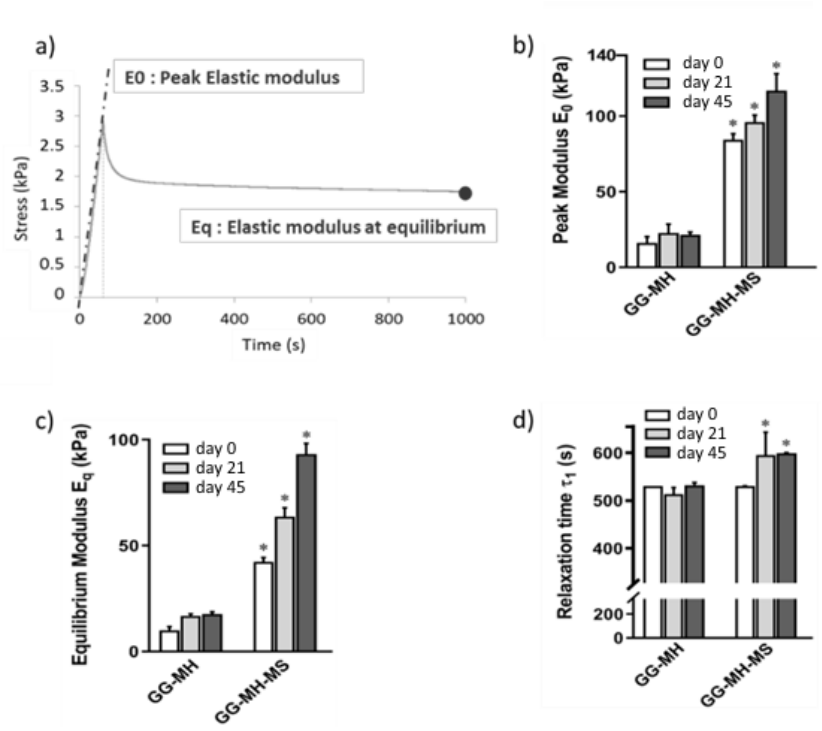


**Figure 7. Stress-relaxation tests.** a) Typical stress-time curve obtained after stress-relaxation tests; b) Peak Modulus $E_0$ values (kPa), calculated from the slope of the initial linear compression ramp; c) Equilibrium Modulus $E_0$ values (kPa), calculated after 1000s and d) relaxation time $\tau_1$(s) calculated by computational analysis of the stress-relaxation curves. Data are presented as mean ± standard deviation. Statistically significant differences with respect to GG-MH are highlighted (*$p<0.01$ versus GG-MH at the same time-point (n=4).

*3.6 In vivo evaluations*

*3.6.1 In vivo immunological reaction*

Fig. 8 describes the mice immunological response to the scaffolds' subcutaneous implants. After 1 week both GG-MH and GG-MH-MS scaffolds did not show evident proofs of immune reaction. Indeed, despite a higher population of splenocytes induced by the presence of the scaffold (Fig. 8a, $p<0.05$ vs control, indicated by *), the T-regulatory cells (T-reg) activity was not decreased by the implants (Fig. 8b). In accordance, starting from a similar % of CD4 positive cells (Fig. 8c), the fully

activated CD8 positive cells increased only in the control group when the infection was introduced (Fig. 8d, $p<0.05$, indicated by *).

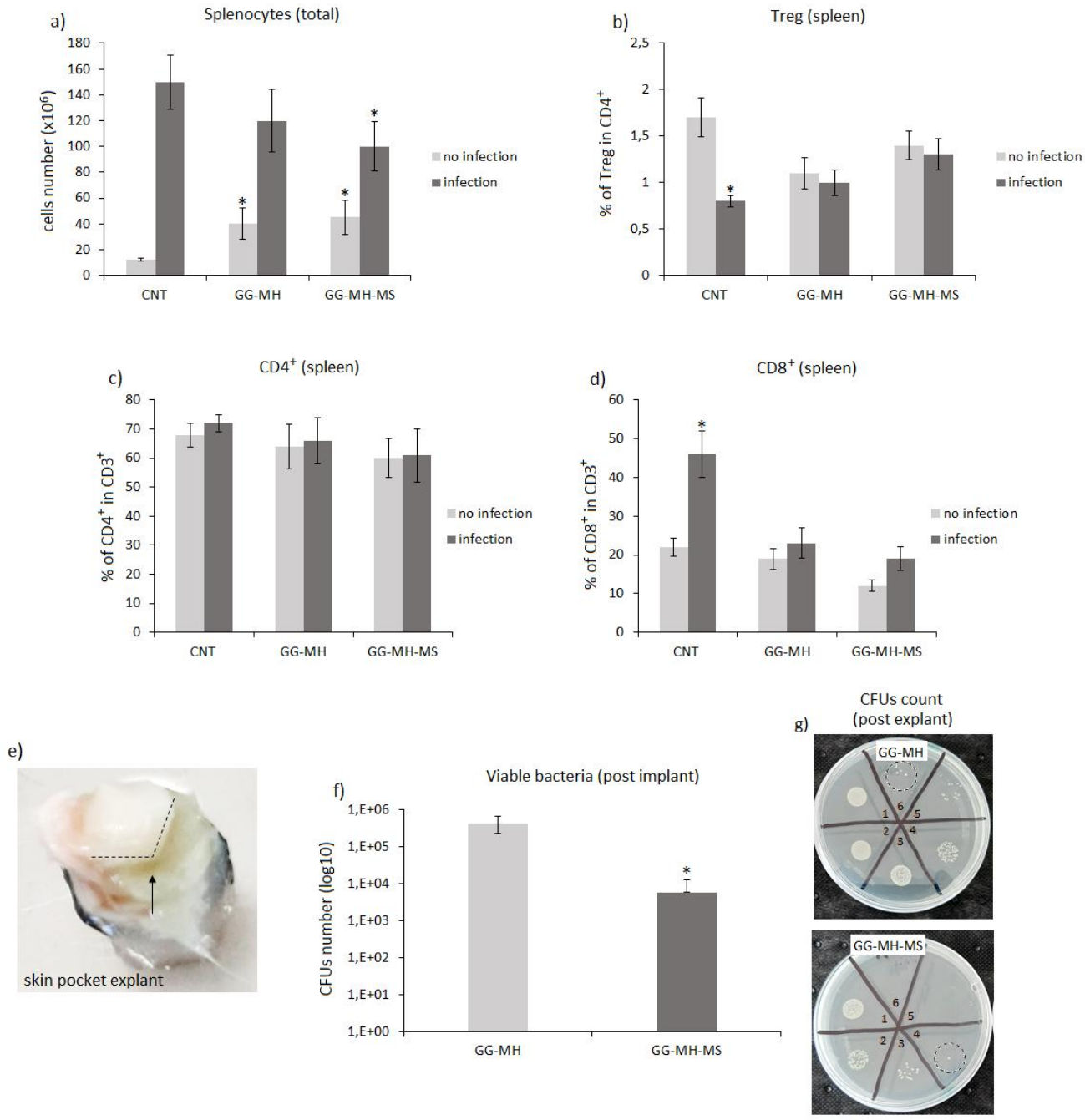


**Figure 8. In vivo biocompatibility and antibacterial assays.** a) total splenocytes population count and b) Treg sub-population count; c-d) cells activation evaluation by means of CD4 and CD8 positive populations; e) representative image of infected explant from GG-MH-MS and f-g) implanted scaffold CFUs count.

*3.6.2 In vivo antibacterial activity*

The prepared scaffolds were infected prior to implantation, in order to test whether they were able to counteract a common bacterial infection. After 1 week, the tissue surrounding the scaffold appeared as

more colonized than the same scaffold (as reported in the representative image of Fig. 8e, scaffold-tissue borders are indicated by the arrows). When the CFUs count was performed (Fig. 8f), it was noticed that the number of bacteria colonizing GG-MH-MS samples was in the same order of magnitude of the initial inoculum ($10^3$ bacteria/scaffold). Therefore, despite the advantageous environment for bacteria, the aforementioned composites were able to contain bacterial proliferation. Moreover, a significant difference was noticed between the two groups (Fig. 8f, $p<0.05$, indicated by *, representative image of bacterial counts on the right) thus suggesting a superior bacteria inhibition from the clay-loaded specimens.

**4. Discussion**

The development of composite scaffolds is a promising strategy to combine the features of different biomaterials, enhancing mechanical, biocompatible and antibacterial performances of the final system. Pursuing this path, the current study describes the preparation of composite scaffolds, based on gellan gum and Manuka honey, including different inorganic clays (HNT, MS or BE). The improvement of gellan-based scaffolds' features can be related to the combination of different parameters, such as the clay's morphology, their dispersion in the hydrogel matrix and the interfacial interactions between inorganic and organic moieties. The three clays exploited in the present work resulted different in chemical composition and, above all, in morphology, ranging from nanotubular (HNT) to lamellar (BE) and to mesoporous (MS) structures. These features are considered to ultimately affect the scaffold's mechanical and biological characteristics. On the other hand, the presence of clays did not alter GG-MH *in vitro* degradation behavior, as previously observed for GG-MH-HNT [11]. In this respect, one of the most common drawbacks of natural polymers is their rapid degradation, not suitable for cartilage repair. The developed scaffolds, by contrast, resulted highly stable *in vitro* (data not shown), even if the mechanisms occurring *in vivo* could be different.

From XPS analysis, the atomic percentages of the analysed hydrogels, reported in Fig.1A, evidenced a typical composition of unreinforced and HNT-reinforced GG-MH systems already analysed in [23], compared with the other systems investigated.

Concerning the organic part of the hydrogel composites, no significant differences in the C1s high-resolution spectra curve fittings (data not shown) were observed as compared to our previous investigations [10, 23]. On the other hand, as far as the inorganic fraction of the clay-reinforced hydrogels was concerned, the analysis of Si2p high-resolution spectra reported in Fig. 1(B-D) revealed a statistically significant decrease (0.55 eV $p<0.05$) in Binding Energy values when MS and BE were included in the hydrogel matrix (Fig.1). This Binding Energy shift could be related to the formation of hydrogen bonds between the oxygen of Si-OH groups belonging to the clays and the COOH and/or OH groups of the organic moieties of the composites [32]. It is likely that little sugars molecules of MH could be intercalated into the cavities of the clays rather than gellan gum polymeric chains. On the other hand, in GG-MH-HNT, the Binding Energy of Si2p did not shift to lower values when these clays were included in the hydrogel matrix, thus excluding any interaction between inorganic and organic moieties, as already observed [23].The incorporation of inorganic clays within the polymeric matrix gave more structural stability and handleability, thanks to a porous morphology. Several works reported that cartilage constructs should provide pores of about 200 μm [33, 34]. Other authors highlighted the need of scaffolds with porosity and microarchitecture similar to the tissue to be regenerated [35]. SEM analysis were performed to evaluate the influence of the inorganic clays' addition on the architecture and porosity of freeze-dried hydrogels (Fig.2). As already reported in literature, the presence of inorganic clays decreases porosity and improves pore walls' thickness [36]. Indeed, the void area, pore area and pore diameter of the clay-containing scaffolds lowered dramatically in comparison with the bare polymeric matrix (Fig.2). The morphology of all the prepared samples suggests that these systems are promising candidates for cell attachment, proliferation and colonization [37]. Furthermore, the presence of micro-porosities (10-30 μm) and thicker pore walls within the clay-reinforced samples allows nutrients absorption and waste transport through the matrix, which are the initial events occurring when a scaffold is placed in biological surroundings [38]. However, the microarchitecture of GG-MH-BE samples displayed lower porosity as compared to GG-MH-HNT and GG-MH-MS

scaffolds. Moreover, pore walls seemed thinner and smoother for GG-MH-BE than the other clay-reinforced samples (Fig.2).

As far as static compression tests are concerned, all the samples showed high values of compression modulus (>100kPa), which are noteworthy if compared with other natural hydrogels for soft tissue and/or cartilage regeneration [39]. The clay-reinforced scaffolds were better than GG-MH samples, in accordance with the previously discussed SEM analysis (Fig.2). This behavior can be attributed to the higher compression resistance of the inorganic clays. Moreover, as previously discussed for the first time by the same authors [10], MH as well plays a key role in the enhancement of the compressive moduli of natural-based hydrogels, leading to more flexible and stable systems. In this work, GG-MH-BE scaffolds showed a higher modulus as compared to the bare organic network. Even if an interaction between the organic network and BE was observed through XPS analysis, the different mechanical performances may be due to the particular morphology and porosity of GG-MH-BE scaffolds rather than the clay-polymer interactions evidenced by XPS analysis (Fig.2). Indeed, the mechanical response is strongly affected by the porosity degree, together with pores size and orientation. Only the hydrogels with MS showed a slight increase in E value (~10-15% more as compared to the other scaffolds) because of the mesostructure typical of this clay [40] and its interaction with the organic network, as demonstrated by XPS characterization and as already described in literature for other MS-reinforced hydrogels [41]. Moreover, the scaffolds showed a compressive Young's moduli consistent with Kelly et al. that reported E values ranging from 100-1000kPa for native articular cartilage [42].

Finally, porosity and mechanical properties should be carefully considered to guide *in vitro* and *in vivo* response, because the mechanical strength is appropriate to maintain pore structure upon implantation, while the pore volume can strongly influence the recruited cell number and the subsequent deposition of new extracellular matrix [43].

After the evaluation of chemical, morphological and mechanical features of the developed scaffolds, these underwent an *in vitro* screening aimed at evaluating their cytocompatibility. Indeed, viability and metabolic activity assays were performed, as well as the qualitative assessment of 3D scaffold

colonization (Fig.4 and Fig.5). In our in vitro experiments with cells, scaffolds were pre-treated with ABM G422 extracellular matrix (ABM®). Indeed, as already reported in literature, a coating of ECM promotes the initial adhesion of cells to the scaffold, especially for polysaccharide-based systems [44, 45]. Ideally, later *in vivo*, the ECM will be reabsorbed and replaced by endogenous ECM secreted by the cells that colonized the scaffold. The highest cell viability was observed on GG-MH-MS samples (Fig.4a). Moreover, after 1 day of culture, metabolic activity of hMSCs was the highest on GG-MH-MS (Fig.4b), suggesting a positive role of MS on hMSCs behavior [37]. To gain further insights into the ability of the different dehydrated scaffolds in promoting cell migration and proliferation in depth, we performed a colonization assay. hMSCs seeded on top of the scaffolds reached their depths only in the case of GG-MH-MS samples (Fig.5 K-O). Conversely, hMSCs showed poor migration activity on the other sample types (Fig.5 A, F, P). The apparent discrepancy between the poor colonization of GG-MH, GG-MH-HNT and GG-MH-BE and the relatively high viability and metabolic activity of hMSC cells grown on them could be explained assuming that, on the former scaffolds, the bulk of cells are not slowed down in their metabolism but only in their migration through the porous matrix. In this respect, the presence of MS might be responsible of the better colonization performance of the GG-MH-MS scaffolds, due to the regular microarchitecture of the resulting composite, which may lead to suitable wettability, protein adsorption and cell-adhesive cues, as reported in [46,47]. Conversely, GG-MH-BE samples failed to provide the same relevant cues for cell attachment. Indeed, bentonite displayed variable behavior on different cell lines [48]. In addition, a "race for the surface" experiment was performed, co-culturing hMSCs and bacteria on the scaffolds (Fig.4 c-d). The exploited bacteria were selected among the most common responsible of joint infections [49], using an inoculum up at $1x10^3$ bacteria, a sufficient amount to determine severe orthopaedic infections [50]. In addition to the well-known antibacterial features of MH, the introduction of clays in these new composites not only effectively increased the scaffold rigidity, but also improved their antibacterial properties. Indeed, it was demonstrated that, differently from mammalian cells, bacteria hardly adapt to irregular surfaces (i.e. nano- or micro-textured surfaces, porous structures), due to the less elastic membrane and to its

higher stability in terms of shape maintenance [51]. In particular, Bernardos et al. (2019) recently reviewed the use of the MS materials to improve antibacterial properties by exploiting it to modify devices nanostructure or as active substances carrier [52]. Finally, it must be considered that 3D cell seeding studies demonstrated that the GG-MH-MS samples were the most effective in preserving stem cells. The latter are intrinsically antibacterial, thus it could be hypothesized that they act as an anti-infective tool. Afterwards, combining the outcomes of all the performed evaluations, a more detailed assessment was focused on GG-MH-MS scaffolds. Thus, hMSCs were cultured in chondrogenic conditions on GG-MH-MS and, as control, on GG-MH scaffolds. Observing histological sections and gene expression profiles, it can be concluded that both GG-MH and GG-MH-MS samples successfully supported chondrogenesis (Fig. 6 b-e). These results are in agreement with previous literature that clearly showed as polymeric hydrogels are very promising materials for cartilage applications (e.g. alginate [53], fibrin glue [54] and methylcellulose [27]). However, PCR showed that GG-MH-MS allowed for a higher expression of ACAN: this is a fundamental finding because ACAN degradation is the hallmark of cartilage degeneration in osteoarthritis (OA) [55]. Therefore, the superior performances of the clay-loaded scaffolds seem to be very promising to avoid one of the better known degradation pathways that lead to OA. Furthermore, before and after chondrogenesis, the scaffolds underwent stress-relaxation tests (Fig. 7). Indeed, it is important to compare the viscoelastic behavior of the prepared hydrogels with that of native tissues, since it affects loads transfer, as well as nutrients diffusion [56]. The results on the as prepared hydrogels confirmed that the incorporation of the inorganic clay increased the mechanical properties with respect to GG-MH hydrogels (Fig. 7a-c), as found for the static compression tests (Fig. 3). Particularly, our stress-relaxation tests were in accordance with Wagenseil et al., that have reported the generalized Maxwell model, consisting in three relaxation times ($\tau1$=1-10s, $\tau2$=10-100s and $\tau3$>500-1000s) allows to model soft biological tissues to evaluate their viscoelastic behavior [57]. The calculated relaxation times (Fig.7d) were comparable with the values reported in literature for polymeric gels and by the same authors in previous works [10,11]. Furthermore, these relaxation times are related with the equilibrium modulus

that was found ~95 kPa for GG-MH-MS, that is in accordance with those reported for native cartilage, which varies with depth from the articular surface [58]. In addition, it has been shown that the mechanical properties (peak modulus, equilibrium modulus, etc.) of cartilage are generally positively correlated to the GAG and COL2 content [59, 60]. Therefore, the enhanced mechanical values of the composite hydrogels can be attributed to the high GAG and COL2 content, as observed from the *in vitro* differentiation tests.

Finally, biocompatibility and antibacterial activity were studied *in vivo*. Materials biocompatibility was verified in terms of immunological reaction of the spleen cells following a foreign body implant by a subcutaneous skin pocket model as previously described [27]. Immunological analysis showed that in absence of infection, implanted scaffolds were recognized by the immune system, since the total number of splenocytes was significantly higher than the PBS control (Fig. 8a). However, both Treg activity and CD4/CD8 staining revealed that most of those cells were not in the activated phase and that the percentage of CD4+CD8 positive cells were comparable in control and implanted groups. Interestingly, when infection was introduced, a strong reaction was recorded in the control animals, in which the Treg anti-inflammatory activity was decreased (Fig. 8b). In addition, the percentage of fully activated CD4+CD8 positive population increased, with the aim to counteract the infection in the absence of antibacterial compounds (Fig. 8c,d). Conversely, splenocytes populations in implanted and infected groups were not significantly changed after infection. These data suggest that the infection was contained by the antibacterial activity of the specimens themselves, thus not requiring a strong activation of the immune system towards bacteria. As a confirmation, the CFU count showed that after 1 week GG-MH-MS presented the same level of viable bacteria of the original infection (in the order of $10^3$/scaffold), thus demonstrating a strong ability to counteract bacterial proliferation, even in a bacteria-rich environment as the subcutis. These results were significant in comparison with GG-MH, that showed an increase of bacteria in the order of about 1 log considering the initial inoculum concentration. The interpretation of these data is not easy, since bacterial reduction is likely due to both the scaffolds and the naïve immune system activity, which act in a cooperative manner. However, the

differences between GG-MH and GG-MH-MS specimens implanted in the same animal model (thus, holding the same immune reactivity) suggest that GG-MH-MS was more effective in counteracting the infection. Accordingly, even if this *in vivo* model does not provide suitable information regarding the materials' ability to promote cartilage repair, as well as the subcutis environment does not resemble the joint one, data suggest that the tested materials are biocompatible and effective in counteracting a possible secondary infection. Furthermore, it has been noticed that these assays were performed in a short-time period (1 week), suitable to observe the early response of the immune system to a foreign body and an eventual infection. This short time did not allow the observation of an *in vivo* degradation. However, here no sample debridement was observed after 7 days from implantation, nor after 45 days of *in vitro* culture, accordingly to previous weight loss experiments [11]. Nevertheless, long-term experiments are required to better understand materials degradation *in vivo*, as well as their ability to support chondrogenesis.

## 5. Conclusions

The reported results highlighted the positive impact of the clays incorporation into the scaffolds' mechanical and morphological features. Even if all the tested inorganic clays significantly improved the scaffolds mechanical properties with respect to the GG-MH system, MS provided the best combination in terms of *in vitro* cytocompatibility, mechanical performances and morphological features. Moreover, for these reasons, GG-MH-MS were further investigated in co-culture, where they preserved hMSCs proliferation over bacteria, as well as they successfully supported the chondrogenic differentiation in a 3D culture model. In addition, MS enhanced the scaffolds' viscoelastic behavior in static conditions and up to 45 days of chondrogenic culture. When implanted in mice, these scaffolds did not cause severe immunological reaction as well as they were effective in enhancing the antibacterial response. Taking into account the mechanical and biological performances of GG-MH-MS scaffolds, the latter show a great potential to address the major challenge of superficial and middle cartilage repair.

## 6. References

[1] L. Yong Ping, W. Xiao Chun, Z. Jing Ming, L. Wei, The age-related changes in cartilage and osteoarthritis, BioMed research international 1 (2013) 1-13.

[2] M. Brittberg, A.H. Gomoll, J.A. Canseco, J. Far, M. Lind, J. Hui, Cartilage repair in the degenerative ageing knee: A narrative review and analysis, Acta orthopaedica, 87 (2016) 26-38.

[3] A.R. Armiento, M.J. Stoddart, M. Alini, D. Eglin, Biomaterials for articular cartilage tissue engineering: Learning from biology. Acta Biomaterialia 65 (2018) 1-20.

[4] G. Balato, S.L. Di Donato, T. Ascione, A. D'Addona, F. Smeraglia, G. Di Vico, D. Rosa, Knee Septic Arthritis after Arthroscopy: Incidence, Risk Factors, Functional Outcome, and Infection Eradication Rate, Joints 2 (2017) 107-113.

[5] C.T. Vangsness Jr, G. Higgs, J.K. Hoffman, J. Farr, P.A. Davidson, F. Milstein, S. Geraghty, Implantation of a Novel Cryopreserved Viable Osteochondral Allograft for Articular Cartilage Repair in the Knee, Journal of Knee Surgery 31 (2018) 528-535.

[6] A. Abazari, N.M. Jomha, J.A. Elliott, L.E. McGann, Cryopreservation of articular cartilage, Cryobiology, 66 (2013) 201-9.

[7] R.M. Jeuken, AK Roth, RJRW Peters, CC Van Donkelaar, JC Thies, LW Van Rhijn, PJ Emans, Polymers in Cartilage Defect Repair of the Knee: Current Status and Future Prospects, Polymers, 8 (2016) 219.

[8] S. Li, S. Dong, W. Xu, S. Tu, L. Yan, C. Zhao, J. Ding, X. Chen, Antibacterial hydrogels, Advanced Science, 5 (2018) 1700527.

[9] H. Liu, Y. Cheng, J. Chen, F. Chang, J. Wang, J. Ding, X. Chen, Component effect of stem cell-loaded thermosensitive polypeptide hydrogels on cartilage repair, Acta Biomaterialia, 73 (2018), 103-111.

[10] M.A. Bonifacio, S. Cometa, A. Cochis, P. Gentile, A.M. Ferreira, B. Azzimonti, G. Procino, E. Ceci, L. Rimondini, E. De Giglio, Antibacterial effectiveness meets improved mechanical properties:

Manuka honey/gellan gum composite hydrogels for cartilage repair, Carbohydrate polymers 198 (2018) 462-72.

[11] M.A. Bonifacio, S. Cometa, A. Cochis, P. Gentile, A.M. Ferreira, B. Azzimonti, G. Procino, E. Ceci, L. Rimondini, E. De Giglio, Data on Manuka Honey/Gellan Gum composite hydrogels for cartilage repair, Data in brief 20 (2018) 831-39.

[12] A. Nahideh, E. Alizadeh, R. Salehi, B. Khalandi, S. Davaran, A. Akbarzadeh, Nanocomposite hydrogels for cartilage tissue engineering: a review, Artificial cells, nanomedicine, and biotechnology, 46 (2018) 465-71.

[13] J.I. Dawson, R.O.C. Oreffo. Clay: new opportunities for tissue regeneration and biomaterial design, Advanced Materials, 25 (2013) 4069-86.

[14] S. Pacelli, P. Paolicelli, G. Moretti, S. Petralito, M.A. Casadei, Gellan gum methacrylate and laponite as an innovative nanocomposite hydrogel for biomedical applications, European Polymer Journal, 77 (2016) 114-123.

[15] H. Lee, B. Rukmanikrishnan, J. Lee, Rheological, morphological, mechanical, and water-barrier properties of agar/gellan gum/montmorillonite clay composite films, International Journal of Biological Macromolecules, 141 (2019) 538-544.

[16] S.S. Mohd, M.A.A. Abdullah, K.A. Mat Amin, Gellan gum/clay hydrogels for tissue engineering application: Mechanical, thermal behavior,cell viability, and antibacterial properties, Journal of Bioactive and Compatible Polymers 2016, 1 –19.

[17] P. Yuan, D. Tan, F. Annabi-Bergaya, Properties and applications of halloysite nanotubes: Recent research advances and future prospects, Applied Clay Science, 112 (2015) 75–93.

[18] G.R.S. Cavalcanti GRS, M.G. Fonseca, E.C. da Silva Filho, M. Jaber, Thiabendazole/bentonites hybrids as controlled release systems, Colloids Surf B Biointerfaces, 176 (2019) 249-55.

[19] A. K. Demir, A.E. Elçin, Y.M. Elçin Strontium-modified chitosan/montmorillonite composites as bone tissue engineering scaffold, Materials Science and Engineering: C, 89 (2018) 8-14.

[20] H. Zheng, F. Gao, V.Valtchev, Nanosized inorganic porous materials: fabrication, modification and application, J. Mater. Chem. A, 4 (2016) 16756-70.

[21] E. Boccardi, L. Liverani, A.R. Boccaccini, Bioactive behavior of mesoporous silica particle (MCM-41) coated bioactive glass-based scaffolds, International Journal of Applied Ceramic Technology, 16 (2019), 1753-1761.

[22] J. Wei, Y. Wang, J. Jiang, Y. Yan, D. Fan, X. Yang, Y. Zuo, Y. Li, H. Gu, J. Li, Development of an Antibacterial Bone Graft by Immobilization of Levofloxacin Hydrochloride-Loaded Mesoporous Silica Microspheres on a Porous Scaffold Surface, Journal of biomedical nanotechnology, 15 (2019) 1097-05.

[23] M.A. Bonifacio, P. Gentile, A.M. Ferreira, S. Cometa, E. De Giglio, Insight into halloysite nanotubes-loaded gellan gum hydrogels for soft tissue engineering applications, Carbohydrate polymers, 163 (2017) 280-91.

[24] G. Kaklamani, D. Cheneler, L.M. Grover, M.J. Adams, J. Bowen, Mechanical properties of alginate hydrogels manufactured using external gelation, Journal of the mechanical behavior of biomedical materials, 36 (2014) 135-42.

[25] B. Martin, S. Tomáš, F. René, Note on the use of different approaches to determine the pore sizes of tissue engineering scaffolds: what do we measure?, Biomedical engineering online, 17(2018) 110.

[26] S. James, J. Fox, F. Afsari, J. Lee, S. Clough, C. Knight, J. Ashmore, P. Ashton, O. Preham, M. Hoogduijn, R.D.A.R. Ponzoni, Multiparameter analysis of human bone marrow stromal cells identifies distinct immunomodulatory and differentiation-competent subtypes, Stem Cell Reports 4 (2015) 1004-15.

[27] A. Cochis, S. Grad, M.J. Stoddart, S. Farè, L. Altomare, B. Azzimonti, M. Alini, L. Rimondini, Bioreactor mechanically guided 3D mesenchymal stem cell chondrogenesis using a biocompatible novel thermo-reversible methylcellulose-based hydrogel. Scientific Reports, 7 (2017) 45018.

[28] I. Ozgol, B.C. Depboylu, A. Tongut, S. Ozdemir, Y. Bagdatlı, S. Ainechi, B. Oz, J.C. Pache, S. Erenturk, A. Kalangos, A.C. Hatemi, M. Cikirikcioglu, Evaluation of Infection Resistance of

Biodegradable versus Conventional Annuloplasty Rings in an in vivo Rat Subcutaneous Model, Eur Surg Res, 58 (2017) 169-179.

[29] K.E. Miller, B. Hontanilla, A. Cabello, D. Marre, L. Armendariz, J. Leiva, The effect of late infection and antibiotic treatment on capsular contracture in silicone breast implants: A rat model, J Plast Reconstr Aesthet Surg, 69 (2016) 70-6.

[30] J. J. Harrison, C.A. Stremick, R.J. Turner, N.D. Allan, M.E. Olson, H. Ceri, Microtiter susceptibility testing of microbes growing on peg lids: a miniaturized biofilm model for highthroughput screening. Nature Protocols 5 (2010) 1236–1254.

[31] L. Bian, D.Y. Zhai, R.L. Mauck, J.A. Burdick, Coculture of Human Mesenchymal Stem Cells and Articular Chondrocytes Reduces Hypertrophy and Enhances Functional Properties of Engineered Cartilage, Tissue Engineering Part A 17 (2011) 1137-45.

[32] H. Liu, D. Chaudhary, S.I. Yusa, M.O. Tadé, Glycerol/starch/Na+-montmorillonite nanocomposites: a XRD, FTIR, DSC and 1H NMR study, Carbohydrate Polymers, 83 (2011) 1591-97.

[33] Q.L. Loh, C. Choong, Three-dimensional scaffolds for tissue engineering applications: role of porosity and pore size, Tissue Eng. Part B Rev., 19 (2013) 485-502.

[34] M.D.B.M. Iliescu, C.D. Hoemann, M.S. Shive, A. Chenite, Ultrastructure of hybrid chitosan–glycerol phosphate blood clots by environmental scanning electron microscopy, Microsc. Res. Tech., 71 (2008) 236-247.

[35] H.-I. Chang, Y. Wang, Cell Responses to Surface and Architecture of Tissue Engineering Scaffolds. In: Regenerative Medicine and Tissue Engineering - Cells and Biomaterials. P.D. Eberli Editor, InTech 2011

[36] A.R. Bastos, L.P. da Silva, F.R. Maia, S. Pina, T. Rodrigues, F. Sousa, J.M. Oliveira, J. Cornish, V.M. Correlo, R.L. Reis, Lactoferrin-Hydroxyapatite Containing Spongy-Like Hydrogels for Bone Tissue Engineering, Materials, 12(2019), 2074.

[37] F.J. O'Brien, Biomaterials & scaffolds for tissue engineering, Mater. Today, 14 (2011) 88–95.

[38] A. Higuchi, S.S. Kumar, Q.D. Ling, A.A. Alarfaj, M.A. Munusamy, K. Murugan, H. Shih-Tien G. Benelli, A. Umezawa, Polymeric design of cell culture materials that guide the differentiation of human pluripotent stem cells, Progress in Polymer Science, 65 (2017) 83-126.

[39] C.W. Peak, J.J. Wilker, G. Schmidt, A review on tough and sticky hydrogels. Colloid and Polymer Science, 291 (2013) 2031-47.

[40] M. Martínez-Carmona, Y. Gun'ko, M. Vallet-Regí, Mesoporous Silica Materials as Drug Delivery:"The Nightmare" of Bacterial Infection, Pharmaceutics, 10 (2018) 279-307.

[41] M. Zhu, Y. Zhu, L. Zhang, J. Shi, Preparation of chitosan/mesoporous silica nanoparticle composite hydrogels for sustained co-delivery of biomacromolecules and small chemical drugs, Science and technology of advanced materials, 14, (2013) 045005.

[42] T.A.N. Kelly, B.L. Roach, Z.D. Weidner, C.R. Mackenzie-Smith, G.D. O'Connell, E.G. Lima, A.M. Stoker, J.L. Cook, G.A. Ateshian, C.T. Hung, Tissue-engineered articular cartilage exhibits tension-compression nonlinearity reminiscent of the native cartilage, Journal of biomechanics, 46 (2013) 1784-91.

[43] J. Kim, W.A. Li, W. Sands, D.J. Mooney, Effect of Pore Structure of Macroporous Poly(Lactide-co-Glycolide) Scaffolds on the in Vivo Enrichment of Dendritic Cells, ACS Applied Materials & Interfaces, 6, (2014) 8505-12.

[44] G. Ramanathan, S. Singaravelu, M.D. Raja, N. Nagiah, P. Padmapriya, K. Ruban, K. Kaveri, T.S. Natarajan, U.T. Sivagnanam, P.T.T. Perumal, Fabrication and characterization of a collagen coated electrospun poly (3-hydroxybutyric acid)–gelatin nanofibrous scaffold as a soft bio-mimetic material for skin tissue engineering applications. RSC Advances, 6 (2016) 7914-7922.

[45] R. Barbucci, Hydrogels: Biological properties and applications, Springer Science & Business Media, 2010.

[46] N. Wang, M. Ma, Y. Luo, T. Liu, P. Zhou, S. Qi, Y. Xu, H. Chen, Mesoporous Silica Nanoparticles-Reinforced Hydrogel Scaffold together with Pinacidil Loading to Improve Stem Cell Adhesion, ChemNanoMat, 4 (2018) 631-641.

[47] S. Yang, J. Wang, H. Tan, F. Zeng, C. Liu, Mechanically robust PEGDA–MSNs-OH nanocomposite hydrogel with hierarchical meso-macroporous structure for tissue engineering. Soft Matter, 8 (2012) 8981-8989.

[48] J. Nones, H.G. Riella, A.G. Trentin, J. Nones, Effects of bentonite on different cell types: A brief review, Applied Clay Science, 105 (2015) 225-230.

[49] N. Benito, M. Franco, A. Ribera, A. Soriano, D. Rodriguez-Pardo, L. Sorlí, G. Fresco, M. Fernández-Sampedro, M. Dolores Del Toro, L. Guío, E. Sánchez-Rivas, A. Bahamonde, ... J. Ariza, Time trends in the aetiology of prosthetic joint infections: a multicentre cohort study. Clinical Microbiology and Infection, 22 (2016), 732-738.

[50] D. Baldoni, U. Furustrand Tafin, S. Aeppli, E. Angevaare, A. Oliva, M. Haschke, W. Zimmerli, A. Trampuz, Activity of dalbavancin, alone and in combination with rifampicin, against meticillin-resistant Staphylococcus aureus in a foreign-body infection model. Int J Antimicrob Agents, 42 (2013) 220-5.

[51] S. Ferraris, A. Cochis, M. Cazzola, M. Tortello, A. Scalia, S. Spriano, L. Rimondini, Cytocompatible and Anti-bacterial Adhesion Nanotextured Titanium Oxide Layer on Titanium Surfaces for Dental and Orthopedic Implants, Frontiers in Bioengineering and Biotechnology, 7 (2019) 103.

[52] A. Bernardos, E. Piacenza, F. Sancenón, M. Hamidi, A. Maleki, R.J. Turner, R. Martínez-Máñez, Mesoporous Silica-Based Materials with Bactericidal Properties, Small, 24 (2019) e1900669.

[53] E. Ruvinov, T. Tavor Re'em, F. Witte, S. Cohen, Articular cartilage regeneration using acellular bioactive affinity-binding alginate hydrogel: A 6-month study in a mini-pig model of osteochondral defects, J Orthop Translat, 16 (2018), 40-52.

[54] O Schätti, S. Grad, J. Goldhahn, G. Salzmann, Z. Li, M. Alini, M.J. Stoddart, A combination of shear and dynamic compression leads to mechanically induced chondrogenesis of human mesenchymal stem cells. Eur Cell Mater, 22 (2011), 214-25.

[55] J.S. Mort, Y. Geng, W.D. Fisher, P.J. Roughley, Aggrecan heterogeneity in articular cartilage from patients with osteoarthritis, BMC Musculoskelet Disord, 17 (2016) 89.

[56] W.J. Marijnissen, G.I. van Osch, J. Aigner, S.W. van der Veen, A.P. Hollander, H.L. Verwoerd-Verhoef, J.A. Verhaar, Alginate as a chondrocyte-delivery substance in combination with a non-woven scaffold for cartilage tissue engineering. Biomaterials, 23 (2002) 1511-17.

[57] J.E. Wagenseil, T. Wakatsuki, R.J. Okamoto, G.I. Zahalak, E.L. Elson, One-dimensional viscoelastic behavior of fibroblast populated collagen matrices, Journal of biomechanical engineering, 125 (2003) 719-25.

[58] Q.T. Nguyen, R.L. Sah, Cartilage-like mechanical properties of poly (ethylene glycol)- diacrylate hydrogels, Biomaterials, 33(2012) 6682–90.

[59] R.L. Mauck, S.L. Seyhan, G.A. Ateshian, C.T. Hung, Influence of seeding density and dynamic deformational loading on the developing structure/function relationships of chondrocyte-seeded agarose hydrogels, Ann Biomed Eng, 30 (2002) 1046-56.

[60] D. Yan, G. Zhou, X. Zhou, W. Liu, W.J. Zhang, X. Luo, L. Zhang, T. Jiang, L. Cui, Y. Cao, The impact of low levels of collagen IX and pyridinoline on the mechanical properties of in vitro engineered cartilage, Biomaterials, 30 (2009) 814-21.